

# An Investigation into the $^{113}\text{Cd}$ Beta Decay Spectrum using a CdZnTe Array

J. V. Dawson,<sup>a</sup> C. Reeve,<sup>b</sup> J. R. Wilson,<sup>c</sup> K. Zuber,<sup>d</sup>  
M. Junker,<sup>e</sup>  
C. Gössling, T. Köttig, D. Münstermann, S. Rajek, O. Schulz<sup>f</sup>

<sup>a</sup>*Laboratoire Astroparticule et Cosmologie, 10 rue Alice Domon et Léonie Duquet,  
75205 Paris, France*

<sup>b</sup>*University of Sussex, Falmer, Brighton. BN1 9QH, UK*

<sup>c</sup>*University of Oxford, Denys Wilkinson Building, Keble Road, Oxford. OX1 3RH,  
UK*

<sup>d</sup>*Institut für Kern- und Teilchenphysik, Technische Universität Dresden,  
Zellescher Weg 19, 01069 Dresden, Germany*

<sup>e</sup>*Laboratori Nazionali del Gran Sasso, Assergi, Italy*

<sup>f</sup>*Lehrstuhl für Experimentelle Physik IV, Technische Universität Dortmund,  
Otto-Hahn Str. 4, 44227 Dortmund, Germany*

---

## Abstract

We present 11 independent measurements of the half-life and spectral shape of the 4-fold forbidden beta decay of  $^{113}\text{Cd}$  using CdZnTe semiconductors with a total combined lifetime of 6.58 kg days. Our overall result gives a half-life of  $(8.00 \pm 0.11(\text{stat}) \pm 0.24(\text{sys})) \times 10^{15}$  years and a Q value of  $322.2 \pm 0.3(\text{stat}) \pm 0.9(\text{sys})$  keV. For the first time half-lives well beyond  $10^{10}$  years have been deduced with a statistically representative sample of independent measurements.

*Key words:*  $^{113}\text{Cd}$  beta decay rare search

*PACS:* 23.40.-s, 27.60.+j

---

## 1 Introduction

In the history of particle and nuclear physics the study of weak interactions and especially beta decay has played a vital role. These studies helped, amongst others, to establish the V-A structure of weak interactions. Nowadays, this interest is somewhat reduced but there are still interesting topics to investigate like the endpoint measurements of tritium and  $^{187}\text{Re}$  electron spectra to determine the neutrino mass [1] or the search for S, T, V contributions to the weak interaction [2]. In addition to these beyond the standard model searches, some interesting nuclear physics questions are still open like the study of highly forbidden beta decays. The major bulk of beta emissions are characterised as allowed or single forbidden, however there are a few isotopes which are at least 4-fold forbidden, having ft-values beyond 20 [3]. These are extremely rare decays with half-lives well beyond  $10^{10}$  years. It occurs that for 5-fold forbidden transitions (like in  $^{48}\text{Ca}$  and  $^{96}\text{Zr}$ ) even double beta decay is more likely to occur.

In this paper the focus is on 4-fold forbidden  $\beta$ -decays. There are only three nuclei in nature which permit a feasible study of four-fold forbidden beta decay,  $^{113}\text{Cd}$ ,  $^{50}\text{V}$  and  $^{115}\text{In}$ , all of them are non-unique ( $\Delta I^{\Delta\pi} = 4^+$ ). Half-lives of these transitions are long ( $\geq 10^{14}$  years) and in typical experiments would produce very low count rates, and as such can only be studied in well shielded, low radioactive background experiments. In this paper the focus is on the decay  $^{113}\text{Cd} (1/2^+) \rightarrow ^{113}\text{In} (9/2^+)$ , with a Q-value of  $320 \pm 3$  keV [4].

The COBRA collaboration is performing a search for neutrinoless double beta decay of which the half-life may be well above  $10^{21}$  years [5]. Results from previous COBRA experiments can be found in [6,7,8]. The present COBRA experiment, known as the 64-array [9], is formed of 64  $1 \text{ cm}^3$  CdZnTe semiconductor crystals, each with a mass of  $\sim 6.5\text{g}$ . The experiment is shielded and situated underground in Laboratori Nazionali del Gran Sasso (LNGS) in Italy. Due to the cadmium content of the semi-conductor, this four-fold forbidden non-unique beta decay of  $^{113}\text{Cd}$  forms the dominant low energy feature. We present results from the first layer of this experiment comprising 16 crystals. Measurements of the half-life of this decay and Q-value have been made independently for 11 working and well-behaved crystals.

There have been five previous attempts to measure the half-life of  $^{113}\text{Cd}$ . The first using a CdTe device resulted in  $(4-12) \times 10^{15}$  years [10]. Measurements using  $\text{CdWO}_4$  as a scintillator found  $7.7 \pm 0.3 \times 10^{15}$  years [11] and as a cryogenic bolometer obtained  $9.0 \pm 0.5(\text{stat}) \pm 1(\text{sys}) \times 10^{15}$  years [12]. Previously the COBRA collaboration obtained  $8.2 \pm 0.2(\text{stat})_{-0.1}^{+0.2}(\text{sys}) \times 10^{15}$  years [13,14] using room temperature CdZnTe semiconductor detectors. A very recent result using a  $\text{CdWO}_4$  scintillator measured  $8.04 \pm 0.05 \times 10^{15}$  years [15]. We present spectra from 11 detectors, with a total exposure of 6.58 kg days.



Fig. 1. First 16 crystal layer inside copper crystal holder during commissioning.

## 2 Experimental Setup

Measurements were performed with the first installed layer of the COBRA 64-array, comprising sixteen  $1 \text{ cm}^3$  CdZnTe semiconductor detectors. The array is housed in an inner copper shield of 5 cm thickness, and surrounded by a lead castle of 20 cm thickness.

The whole setup is enclosed in a Faraday cage, which itself is surrounded by a neutron shield made out of 7 cm thick boron-loaded polyethylene plates and 20 cm of paraffin wax. The full experiment is situated in Laboratori Nazionali del Gran Sasso (LNGS) with 1400 m of rock shielding, corresponding to about 3500 metres water equivalent.

The CdZnTe detectors were manufactured by eV-PRODUCTS [16], and are CoPlanar Grid (CPG) devices[17] with gold anode grids and cathode. Detectors of this kind only read out the electron signal and their operational principle is analogous to a Frisch grid in a wire chamber. The detectors are coated with a passivation paint to provide a highly resistive surface layer and to maintain longterm stability. The detectors are bonded to kapton signal and high voltage foils with a low activity copper loaded glue which was developed in-house. Each crystal receives individually tailored high voltage, grid bias and weighting of the CPG subtraction circuit. These parameters are optimised to minimise the Full Width Half Maximum of the 1274.5 keV photopeak from a  $^{22}\text{Na}$  calibration source. The CPG guard rings are not contacted to maximise the active mass of each crystal, typically 6.5g. Each crystal has a slightly different mass, which are known having being weighed by the manufacturers prior to passivation; Table 1.

All the COBRA electronics have been designed and manufactured in-house. The CPG anode signals are processed by a 16-channel preamplifier based on the suggested circuit from eV-PRODUCTS. The resulting signals are shaped by COBRA shaping amplifiers with time constants of  $1\mu\text{s}$ , digitised by COBRA four-channel 14-bit peak sensing ADCs which are integrated into VME architecture. The manufacturer (Analog Devices) specifications of the 14-bit

peak sensing ADC chip, AD7865 [18], give a maximum DNL (Differential Non-Linearity) of  $\pm 1$ LSB (Least Significant Bit). All ADCs have a slight variation on the width of each ADC code (voltage range which results in a particular ADC code) and this can be observed in spectra with high numbers of counts, such that the Poisson uncertainty is insignificant in comparison with the variation of each ADC code width. The resulting effect on a spectrum is that neighbouring ADC values appear to be statistically incompatible with each other. These effects are not confused for real spectral features since the former occur on a bin-by-bin basis, and spectral features are usually far wider. In some situations this effect can be considered as a systematic or indeed calibrated for. If, as in this case, spectra from different ADCs or with different calibrations as with a long running experiment are summed energy-wise then the effect becomes statistical. It was found that an assumption of an uncertainty of 10% on each ADC code was enough to bring neighbouring values into statistical agreement for the whole COBRA dataset. All data-sets presented, therefore, have statistical uncertainties that include a 10% uncertainty on the bin-width. For low statistics data-sets, such as for double-beta decay studies, the number of counts are too low to observe this effect and only the study of the  $^{113}\text{Cd}$  spectrum is affected.

The COBRA setup is regularly calibrated with  $^{22}\text{Na}$  (511 and 1274.5 keV photopeaks),  $^{57}\text{Co}$  (122.1 keV photopeak) and  $^{228}\text{Th}$  (2614.5 keV photopeak) sources. A linear relationship between energy and ADC channels is found. Independent confirmations of the external calibration are made by measuring photopeaks present in the combined low background spectrum. Two prominent photopeaks are observed in the low background data, at  $351.2 \pm 0.9$  keV and  $606 \pm 2$  keV, these are identified as the 351.9 keV and a blend of 609.3 keV and 583 keV lines from the  $^{238}\text{U}$  and  $^{232}\text{Th}$  chains. We take the uncertainty on the 351.9 keV line, 0.9 keV, as a representation of the systematic uncertainty of the energy calibration of the entire experiment. This peak is close to the  $^{113}\text{Cd}$  shoulder and is therefore a very relevant calibration point. It was observed through-out the entire duration of the experiment and so if any calibration drifts did occur it would be subject to the same bias as the data. The uncertainty on the peak position is slightly greater than the bin-width of the spectra, 0.7 keV, and is probably dominated by the number of counts observed, and therefore can be considered as a conservative estimate.

The relationship between the energy resolution (quantifiable in terms of Full Width Half Maximum) and photopeak energy is found to closely follow the functional form  $FWHM = \sqrt{a^2 + (b.E)^2}$ , where a and b are fit parameters. Table 1 shows these resolution equations determined for the operational detectors. Runs were taken in units of 1 hr. Hour-long runs were deemed abnormal and rejected from the analysis if the number of counts observed in that run did not conform to the overall observed mean count rate. If the probability of the count rate for each hour-long run being compatible with the mean count rate was lower than 1% then that run was rejected from the analysis. Such

runs on closer inspection showed rapid bursts of events, thought to be due to vibrations, micro-discharges on the high voltage cables and electronic effects.

### 3 Background Model

As common in rare event searches a background model can be constructed. This is based on the measurement of radioactive contaminants in material samples. This typically includes the natural decay chains of U and Th,  $^{40}\text{K}$  and potential isotopes produced by cosmic ray spallation while the materials were on surface. With the given activities a theoretical spectrum can be constructed which should agree with the observable spectrum if all impurities are included. To account for detector effects, the background spectrum for the experiment is simulated using a GEANT 4 based simulation code. This simulation includes the 16 crystals with passivation paint, delrin crystal holder, copper and lead shielding.

In our case, the detector components have been assessed by the LNGS low background counting facility. Table 2 shows the overall results. Only the passivation paint which coats 5 sides of each crystal has definitive measurements, all the rest are upper limits. This passivation paint is anticipated to be a major background contributor to the experiment.

Figure 2 shows the summed background spectrum from all 11 crystals (higher rate spectrum with error bars). The dominant low energy feature (below  $\sim 320$  keV) is the beta decay spectrum of  $^{113}\text{Cd}$ , a theoretical spectrum is shown (dot dashes). Superimposed on top of this are background spectra arising from contaminants in the local environment.

The main identified contaminants are radon gas, and trace uranium and thorium found in the crystal passivation coating. Simulations of these contaminants have been made and are shown in Figure 2 (small squares and dashes). To address this issue new crystals with a colourless passivation coating were purchased and briefly operated in the shielded setup. This new coating was tested in the LNGS low counting facility, and is far cleaner than the one coating the 16-crystals, with only upper limits found,  $<34$  ppm  $^{40}\text{K}$ ,  $<11$  ppb  $^{238}\text{U}$  and  $<45$  ppb  $^{232}\text{Th}$ . The spectrum obtained with one colourless crystal is shown in Figure 2 (square data points with error bars).

Of equal concern is the presence of radon gas inside the inner detector volume. The experiment has recently been moved from the outer parts of LNGS laboratory to a new location between the main halls A and B (which is known to be less abundant in radon), and as a result the overall background count rate has fallen. Brief experimentation with flushing with nitrogen boil-off gas from a liquid nitrogen dewar and filtering with a radon filter has shown improvements in background rates, supporting the hypothesis that radon gas is observable in the background spectrum. The spectrum from the new colourless

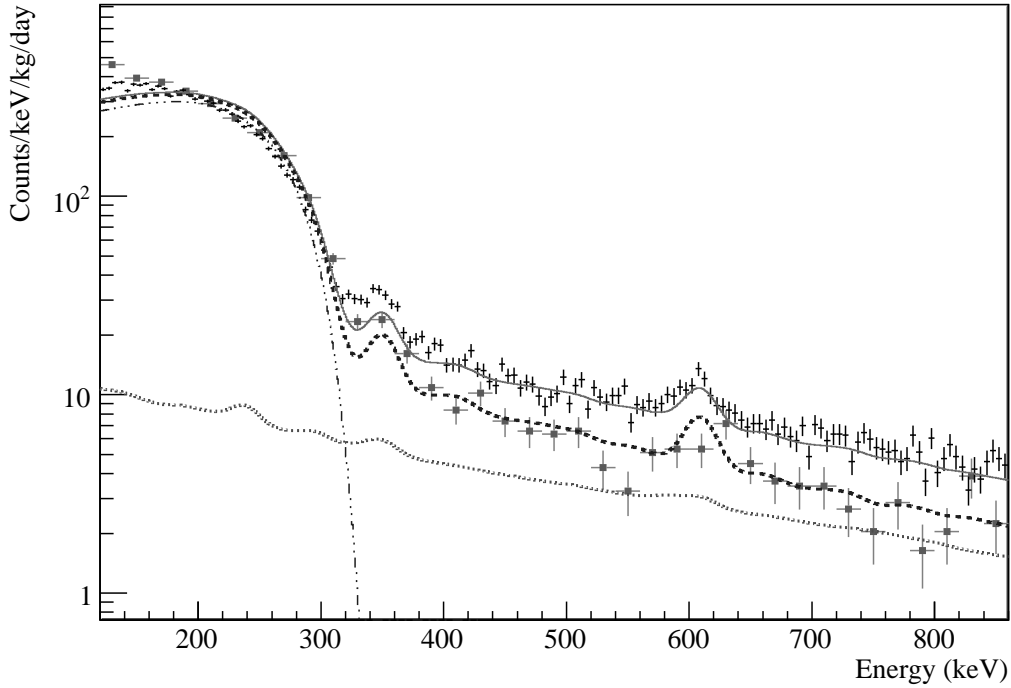


Fig. 2. Summed spectrum from all detectors (higher rate spectrum with error bars), compared to crystal with new passivation coating (square marker with error bars). Overlaid are the simulated backgrounds produced by the passivation coating (light dashes) and theoretical  $^{113}\text{Cd}$  beta spectrum (dot-dashes). The effect of radon gas and combined with the  $^{113}\text{Cd}$  beta spectrum (bold dashes), overlaps the data from the new crystals. The sum of these components (thin continuous line) overlaps the spectrum from all detectors. The 351.9 keV and 609.3 keV  $\gamma$ -lines from the  $^{238}\text{U}$  decay chain are visible in the spectrum.

crystals showed far less of a reduction in background than anticipated from the contamination measurements. Their spectrum is assumed to be dominantly contaminated by radon. In effect these measurements give the radon contamination levels. Simulated  $^{222}\text{Rn}$  in the air cavity of the inner detector volume is shown in Figure 2 (dashes) as well, and is scaled to fit the colourless data.

Finally the sum of these components; paint contamination and radon, and the theoretical  $^{113}\text{Cd}$  spectrum, is shown in Figure 2 (thin continuous line).

The simulated paint spectrum is blended with the energy resolution of each detector and the resulting spectrum is subtracted from each real data spectrum. The radon levels are unknown and may also change over time and so could be different for each detector. However, as can be seen in Figure 2 the Rn level is basically given by the measured spectrum of the colourless painted detector and has a small effect on the total rate of the  $^{113}\text{Cd}$  spectrum as described in more detail later. The simulated radon spectrum is blended with the energy resolution of each detector and the resultant spectrum is fitted to the

real data spectrum with the range 350 to 700 keV. If the background is known and the simulation accurately represents the experiment, then each real data spectrum should consist only of the contribution from the  $^{113}\text{Cd}$  spectrum. These 11 spectra are then used to determine the Q value and half-life of the  $^{113}\text{Cd}$  spectrum.

## 4 Sources of Systematic Uncertainties

The following subsections describe the main sources of systematic uncertainties. Table 3 shows the comparison between the differing effects. The dominant sources of systematic uncertainty are the cadmium content and the energy calibration. The uncertainties are asymmetric since the deadlayer contribution can only reduce the crystal mass. We assume that these uncertainties are independent and therefore add them quadratically to obtain the total uncertainty of  $+2.9, -3\%$ . As we have many detectors we can attempt to estimate the systematic uncertainty, see Section 8.

In the collaboration's previous attempt to measure the  $^{113}\text{Cd}$  half-life [14], the largest source of uncertainty came from the uncertainty in the detector deadlayer. This has now been improved and it can be shown that this systematic was previously heavily over-estimated.

### 4.1 Cadmium Content and crystal mass

CdTe semiconductors are well known to suffer from polarisation problems. This issue was addressed with the addition of zinc, such that CZT detectors are of the form  $\text{Cd}_{1-x}\text{Zn}_x\text{Te}$  with a proportion of zinc,  $x$ , typically of 0.1. Due to the production method, boules of material are grown and the crystals cut from this. The zinc quantity can be non-uniform throughout the entire boule such that detectors cut from one part may not have the same zinc content as crystals cut from another, and hence there exists a systematic uncertainty on the corresponding quantity of cadmium in each crystal. Based on advice from the manufacturers, the zinc admixture was assumed to be between 7-11%, such that the proportion of cadmium could be between 89-93%. Since all the detectors are different and could have come from different locations in the boule we therefore assume an average value of 91% to calculate the half-life for each crystal, and include a systematic uncertainty of 2% in the half-life. The mass measurements per crystal, as given by the manufacturers, are shown in Table 1 and are assumed to have an uncertainty of 0.001 g, or 0.015%

## 4.2 Crystal Deadlayer

It is possible that the crystals possess an inactive layer of CdZnTe, thus reducing the effective mass of the detectors. Observations of alpha signals from an  $^{214}\text{Am}$  source with peak alpha energy of 5.5 MeV penetrating all sides of a painted CZT crystal indicate that if deadlayers exist they are of the order of  $\sim 15\mu\text{m}$ , and can not be substantially larger. The presence of a deadlayer of the order of  $15\mu\text{m}$  would reduce the amount of active mass of the detectors by 0.9%.

## 4.3 Detection Efficiency

As the CdZnTe detectors are small ( $1\text{ cm}^3$ ) some proportion of the  $^{113}\text{Cd}$  betas will escape the detector without fully depositing their energy, slightly distorting the observed spectrum. Complete escapes are also possible. Using the COBRA simulation tool  $^{113}\text{Cd}$  betas were simulated uniformly throughout a crystal volume and the resulting spectrum compared to the theoretical spectrum used. For a threshold of 120 keV, the probability of observing a  $^{113}\text{Cd}$  beta compared to the theoretical spectrum is found to be 0.9932. So we can anticipate that 0.68% of the betas escape or deposit less energy than 120 keV in each detector. This efficiency must be factored into the total half-life estimate. The uncertainty on this quantity is assumed to be 0.0002.

## 5 Background Subtraction

The background is assumed to be due to known quantities as discussed earlier in Section 3. The background level is anticipated to be slightly different for each crystal and each data set as radon levels fluctuate with time. The systematic uncertainty on the half-life from this component is calculated from the uncertainty on the background model fit to each spectrum. Table 4 details the amount subtracted from the spectrum, assumed to be background, and the residual spectrum which is assumed to be a pure  $^{113}\text{Cd}$  spectrum. Some  $\sim 10\%$  of the data are removed from each spectrum in this process within the range 120 to 320 keV. Typically the uncertainty on the background fit is  $\sim 6\%$ . Therefore the systematic uncertainty on the number of counts in the pure  $^{113}\text{Cd}$  spectrum is estimated to be 0.58%.

## 5.1 Energy Calibration

The estimation of the systematic uncertainty based on the energy calibration was made using the summed spectrum of all 10 detectors. The observed 351.9 keV line, from the  $^{238}\text{U}$  chain, was fitted with a Gaussian function returning a mean energy of  $351.2 \pm 0.9$  keV. This line was used as it is the closest photopeak to the falling edge of the  $^{113}\text{Cd}$  spectrum. The falling edge of the beta spectrum highly constrains the fit, so the energy calibration of this feature is the most important. We assume, therefore, that the energy calibration is good to at least 0.9 keV. The fit procedure described in the following section was repeated with spectra shifted (both in the positive and negative senses) by 0.9 keV. The normalisation and hence the half-life changed by  $\pm 2\%$ .

## 6 Fit Method

The shape of the beta spectrum is theoretically described as

$$N(E) = F(Z, E) \cdot p(E + m_e) \cdot (Q - E)^2 \cdot S(E) \quad (1)$$

where  $F(Z, E)$ , the Fermi function is interpolated from tabulated values found in [19]. Here the electron momentum is  $p(E)$ , mass  $m_e$  and kinetic energy  $E$ , and  $Q$  is the endpoint of the beta decay spectrum.

Following the approach of [11] the correction factor,  $S(E)$ , is assumed to be

$$S(E) = p(E)^6 + 7 \cdot c_1 \cdot p(E)^4 \cdot q(E)^2 + 7 \cdot c_2 \cdot p(E)^2 \cdot q(E)^4 + c_3 \cdot q(E)^6 \quad (2)$$

where  $q(E)$  is the neutrino momentum. This form is for a four-fold unique beta decay, but has been found to fit the observed spectrum well by many authors [6,11,15].

The energy resolution of the detectors smears the spectrum, but as the detector resolution changes with energy, it was necessary to use Monte Carlo techniques to simulate test spectra and perform chi-squared fits to the data. The assumed resolutions and functions are described in Section 2. A MINUIT routine was devised, with the following free parameters

- $Q$  - the  $Q$  value of the beta transition.
- The spectral  $S(E)$  parameters;  $c_1$ ,  $c_2$  and  $c_3$ .
- The amplitude of the spectrum which is related to the half-life

To determine the half-life for each crystal the outputted fit parameters were used to determine the integral number of counts between 0 and the determined  $Q$  value. As each parameter has an associated uncertainty, including the  $Q$  value, Gaussian random deviates were drawn to give estimates of each parameter and the resulting beta spectrum integrated. This procedure was repeated for each detector 1000 times, and the determined integral counts averaged. The standard deviation of this distribution represents the uncertainty

on the integral due to the uncertainties on the fit.

The half-life was calculated according to:  $T_{\frac{1}{2}} = \ln(2)\eta_{det}N\frac{t}{S}$ , where the efficiency  $\eta_{det}$  is the efficiency of detecting a beta decay,  $N$  is the number of source  $^{113}\text{Cd}$  atoms,  $t$  is the measuring time and  $S$  is the total number of counts in the beta spectrum. Since we do not measure the entire beta spectrum, energy thresholds are typically  $\sim 100$  keV,  $S$  is the integral of the fitted spectrum from 0 keV to the determined Q-value. The efficiency  $\eta_{det}$  accounts for the fact that some betas above the energy threshold escaped, reducing the number of counts in the observed spectrum. This value was taken as 0.9932 (as discussed in Section 4.3). The number of  $^{113}\text{Cd}$  source atoms is calculated for each detector, and assumes a natural abundance of  $^{113}\text{Cd}$  isotope of 12.22(12)% [20] and the overall proportion of cadmium with respect to zinc to be 0.91 (as discussed in Section 4.1).

## 7 Results

Each spectrum was fitted individually with a theoretical  $^{113}\text{Cd}$  spectrum over the range 100 to 350 keV. If the goodness-of-fit probability was low (less than 0.1) then the low energy threshold was raised to 150 keV. The fit range, which passes the expected endpoint of the spectrum, is necessary to establish that the residual background is consistent with 0. Above 150 keV we are confident that the background model accurately describes the data, and therefore the background subtraction is valid.

The Q value and spectral parameters ( $c_1$ ,  $c_2$  and  $c_3$ ) should be the same for each detector since they describe the shape of the beta spectrum. Previous estimates of the spectral shape parameters have been measured by other authors:  $c_1 = 1.01 \pm 0.01$ ,  $c_2 = 1.48 \pm 0.05$ ,  $c_3 = 0.68 \pm 0.21$ [11],  $c_1 = 0.765 \pm 0.095$ ,  $c_2 = 0.589 \pm 0.177$ ,  $c_3 = 2.04 \pm 0.74$ [12] and  $c_1 = 1.016 \pm 0.005$ ,  $c_2 = 1.499 \pm 0.016$ ,  $c_3 = 3.034 \pm 0.045$  [15].

A first attempt at fitting all the spectra resulted with a best estimate of Q as  $323 \pm 0.4$  keV with  $c_1 = 0.97 \pm 0.03$ ,  $c_2 = 3.14 \pm 0.04$  and  $c_3 = -0.33 \pm 0.02$ . Only the value of  $c_1$  measured here is consistent with these previous measurements. The reason being that  $c_2$  and  $c_3$  especially are highly dependent on the behaviour at low beta energies. The threshold in this work is too high to well constrain these parameters.

A recent publication by [15] gives a well measured beta spectrum of  $^{113}\text{Cd}$  down to 30 keV with the best uncertainties on the spectral parameters,  $c_1 = 1.016 \pm 0.005$ ,  $c_2 = 1.499 \pm 0.016$ ,  $c_3 = 3.034 \pm 0.045$ . The 11 spectra were re-fitted using these spectral shape values as inputs rather than as free-floating parameters. The uncertainties on each spectral parameter were used to ascertain the uncertainties on the half-life in the procedure described in 6. The fits are shown in Figure 3.

Table 5 shows the outputted fit parameters and their uncertainties. In this scenario the weighted mean Q value is  $322.2 \pm 0.3(stat)$  keV. Table 6 shows the resulting half-lives determined from this fit. Weighted means of these half-lives give a new estimate of  $^{113}\text{Cd}$  half-life as  $(8.00 \pm 0.11(stat)) \times 10^{15}$  years.

## 8 Discussion

We have made the most numerous measurements of 4-fold forbidden beta decays in this case for  $^{113}\text{Cd}$ , using 11 independent CdZnTe detectors. Each can have a unique (and independent) set of detector parameters such as energy resolution, mass and  $^{113}\text{Cd}$  content etc. This gives a clear cross-check on our estimate of total systematic uncertainty. Figure 4 shows a histogram of the half-lives determined for each detector. The spread in these results must be consistent (or at least smaller than) the combination of the estimated total systematic uncertainty and the determined statistical errors. The total systematic uncertainty was estimated earlier in Section 4 to be  $\sim 3\%$ .

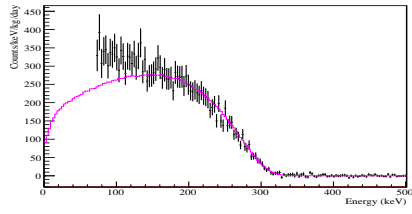
The statistical uncertainties on each half-life are derived from the fits and are shown in Table 6. The weighted mean uncertainty is  $1.1 \times 10^{14}$  years which is 1.3% of the weighted mean half-life. Assuming the systematic and statistical uncertainties are independent, we would therefore expect the distribution of the half-lives shown in Figure 4 to have a standard deviation of  $\sim 3.3\%$ .

As can be seen in Figure 4, all the half-life estimates cluster except for two results which are well separated from the rest of the data. These are from detectors 10 and 11, which both show significant low energy features and displayed bad goodness-of-fit probabilities when fitted with the low energy threshold of 100 keV. If these two detectors are ignored then the remaining estimates give an overall half-life value of  $(7.9 \pm 0.3) \times 10^{15}$  years. The total uncertainty found is therefore 4% of the mean value. This uncertainty is larger than our estimates, 3.3%, but not unreasonably so. It may indicate that we have underestimated one of our systematic errors. One clear possibility to explain this discrepancy could be the assumed spread in the cadmium content since we have as yet no independent measurements of the content of these detectors.

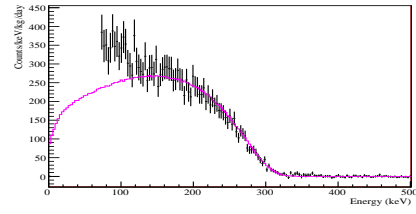
The estimate of the Q-value is dependent on the fitted function, and assuming the used functional form to be correct, is found to be  $322.2 \pm 0.3(stat) \pm 0.9(sys)$  keV. Interestingly the work of [15] fails to fit a feasible Q-value that is consistent with the Table of Isotopes value of  $320 \pm 3$  keV [4].

Encouraged by the results of [14] for the first time microscopic models were explored to predict the half-life and spectral shapes of 4-fold forbidden non-unique beta decays [21]. The measured spectrum of one of the detectors, our fitted spectrum and this theoretical calculation are shown in Figure 5. The

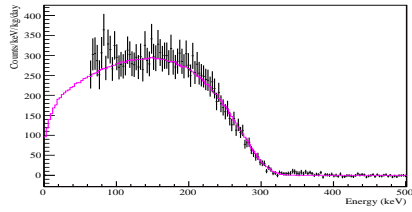
Fig. 3.  $^{113}\text{Cd}$  spectra and fit with  $c_1, c_2$  and  $c_3$  fixed.



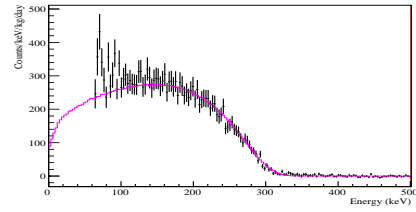
(a) Detector 2



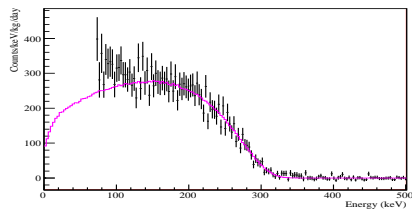
(b) Detector 3



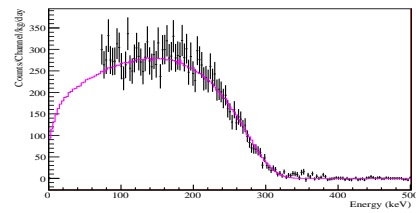
(c) Detector 5



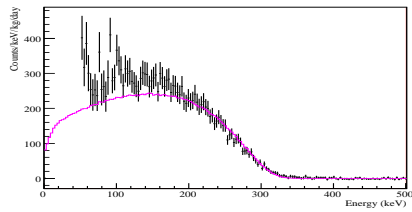
(d) Detector 7



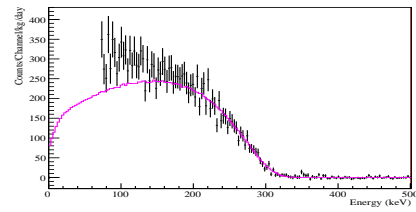
(e) Detector 8



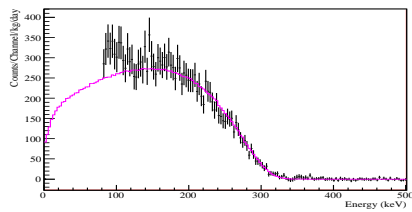
(f) Detector 9



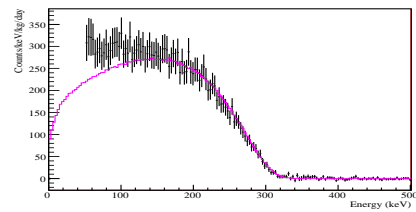
(g) Detector 10



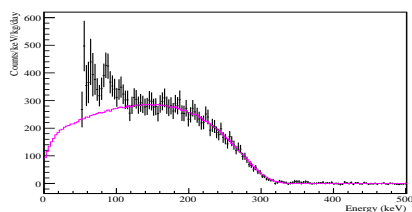
(h) Detector 11



(i) Detector 12



(j) Detector 14



(k) Detector 15

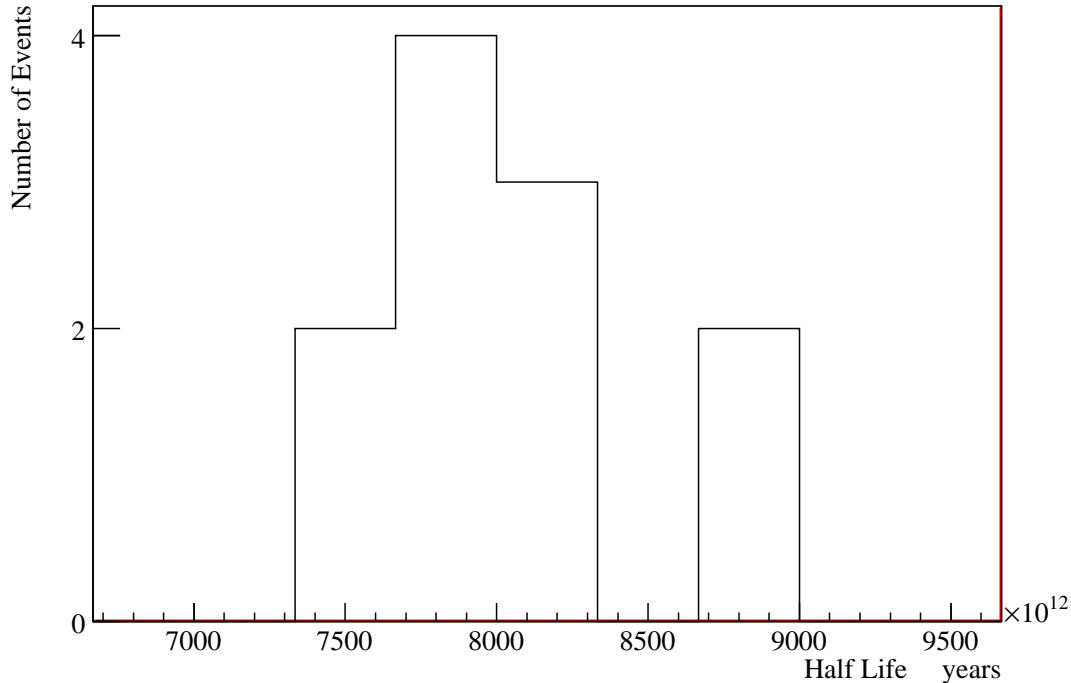


Fig. 4. Histogram of the determined half-lives for all 11 detectors.

theoretical calculation assumed a Q-value of 320 keV. The spectral shape we measure does not match well with the theoretical spectrum and instead agrees well with the 4-fold forbidden unique spectrum as shown by [15]. This is an interesting result and will hopefully motivate some further investigation as to why the fit for a unique transition, normally only linked to one nuclear matrix element fits better than the actual non-unique calculation.

## 9 Conclusion

CdZnTe semiconductor detectors were used to search for the rare decay of the 4-fold forbidden non-unique beta decay of  $^{113}\text{Cd}$ . For the first time a statistically relevant sample of half-life measurements have been obtained for such rare decays. We confirm that the parameterisation of [15] is a good fit to our data above 100 keV. Using this parameterisation we obtain an estimate of the Q-value of the decay to be  $322.2 \pm 0.3(\text{stat}) \pm 0.9(\text{sys})$  keV. Assuming the fit to the data is correct, the resultant half-life is  $(8.00 \pm 0.11(\text{stat}) \pm 0.24(\text{sys})) \times 10^{15}$  years which is completely consistent with previous measurements.

Future work will improve upon the background levels experienced by the experiment. Short test runs with four lower background detectors (with colourless passivation coatings) have already been made. These new runs also fea-

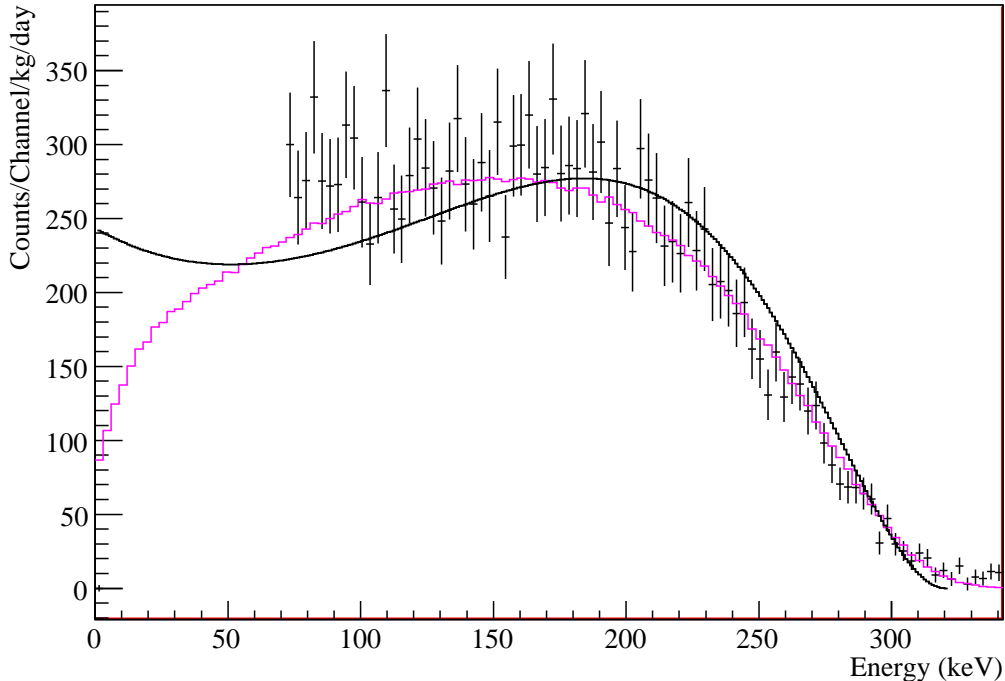


Fig. 5.  $^{113}\text{Cd}$  spectra from Detector 9 showing fit (histogram), and microscopic calculation of [21] (smooth line). Despite the fact that the major effect occurs in the low energy behaviour a discrepancy is already visible at the high energy end. This is true in all measured spectra. The parameterisation of [15] is a good fit to the data above 100 keV.

tured a clean nitrogen flushing system which reduces significantly the radon level in the shielded setup. Longer runs are required to improve on the current result. Ideally a new long run with many colourless detectors would be done, allowing the same systematic cross-checking that has been done in this experiment.

As shown in Figure 3 there are some unexplained background features below 100 keV that are present on most but not all of the detectors. Future work will try to ascertain where this background comes from.

Applying mild cooling ( $\sim 10^\circ\text{C}$ ) to the detectors whilst inside the shielded setup will also be explored. This will reduce the surface leakage current dramatically and therefore lower the energy threshold and improve the energy resolution [22].

Non-intrusive means of measuring the zinc content are already being explored e.g. photoluminescence and X-ray fluorescence techniques. However, these techniques must be applied to the crystals in use either before bonding or at the end of the science run.

## Acknowledgements

We thank our COBRA colleagues for their support. J Wilson acknowledges the support of the Leverhulme Trust. We are grateful to J. Suhonen for providing a data file with the expected beta spectrum based on microscopic calculations.

## References

- [1] J. Bonn, *AIP Proc. Conf.* **972**, 404 (2008).
- [2] N. Severijns, M. Beck, O. Naviliat-Cuncic, *Rev. Mod. Phys.* **78** 991 (2006).
- [3] B. Singh et al., *Nucl. Data Sheets* **84**, 487 (1998).
- [4] G. Audi, A. H. Wapstra and C. Thibault, *Nucl. Phys. A* **729**, 337 (2003).
- [5] K. Zuber, *Phys. Lett. B* **519** 1 (2001).
- [6] H. Kiel et al, *Nucl. Phys. A* **732** 499-514 (2003).
- [7] D. Münstermann, K. Zuber, *Journ. Phys. G* **B1**, 29 (2003).
- [8] T. Bloxham et al., *Phys. Rev. C* **76** 025501 (2007).
- [9] D. Münstermann, Ph. D. Thesis, Technische Universität Dortmund, (2007).
- [10] L. Mitchell and P. Fischer, *Phys. Rev. D* **38**, 895 (1988).
- [11] F. Danevich et al., *Phys. Atom. Nucl.* **59**, 1 (1996).
- [12] A. Alessandrello et al., *Nucl. Phys. B Proc. Suppl.* **35**, 394 (1994).
- [13] H. Kiel, Ph. D. Thesis, Technische Universität Dortmund, <http://hdl.handle.net/2003/21509> (2005).
- [14] C. Goessling et al, *Phys. Rev. C* **72**, 064328 (2005).
- [15] Belli et al, *Phys. Rev. C* **76**, 064603 (2007).
- [16] eV-PRODUCTS, <http://www.evproducts.com> .
- [17] P. Luke, *IEEE Trans. Nucl. Sci.* **42**, 4 (1995).
- [18] Analog Devices, <http://www.analog.com>
- [19] H. Behrens and J. Janecke, *Numerical Tables for Beta Decay and Electron Capture*, Springer Publ., Berlin (1969).
- [20] National Nuclear Data Center, information extracted from the Chart of Nuclides database, <http://www.nndc.bnl.gov/chart/>
- [21] M.T. Mustonen, and J. Suhonen, *Phys. Lett. B* **657**, 38 (2007).
- [22] J. V. Dawson et al, *accepted Nucl. Inst. Meth. in Phys. Res. A*, doi:10.1016/j.nima.2008.11.013 (2008).

Table 1

Detector properties: mass of crystals, and FWHM resolution equations in keV with  $E$ , energy, in keV.

Detector	Mass(g)	Resolution Equation
1	6.483	none
2	6.454	$\sqrt{((13.261 \pm 0.196)^2 + ((0.02843 \pm 0.0003)E)^2)}$
3	6.454	$\sqrt{((10.616 \pm 0.301)^2 + ((0.02714 \pm 0.0003)E)^2)}$
4	6.524	none
5	6.512	$\sqrt{((10.037 \pm 0.239)^2 + ((0.02373 \pm 0.0002)E)^2)}$
6	6.459	none
7	6.526	$\sqrt{((20.649 \pm 0.156)^2 + ((0.02964 \pm 0.0003)E)^2)}$
8	6.465	$\sqrt{((13.937 \pm 0.636)^2 + ((0.04718 \pm 0.0006)E)^2)}$
9	6.469	$\sqrt{((10.502 \pm 0.254)^2 + ((0.02638 \pm 0.0003)E)^2)}$
10	6.461	$\sqrt{((48.588 \pm 2.950)^2 + ((0.07473 \pm 0.0041)E)^2)}$
11	6.468	$\sqrt{((14.673 \pm 0.303)^2 + ((0.03786 \pm 0.0004)E)^2)}$
12	6.492	$\sqrt{((11.570 \pm 0.317)^2 + ((0.02639 \pm 0.0004)E)^2)}$
13	6.529	$\sqrt{((33.630 \pm 1.824)^2 + ((0.05804 \pm 0.0023)E)^2)}$
14	6.548	$\sqrt{((11.672 \pm 0.243)^2 + ((0.02384 \pm 0.0003)E)^2)}$
15	6.520	$\sqrt{((10.703 \pm 0.395)^2 + ((0.02771 \pm 0.0005)E)^2)}$
16	6.509	none

Table 2

List of Contaminants

Material	Isotope	Activity (g/g)
Copper	Th-232	$< 5.7 \times 10^{-10}$
	U-238	$< 2.0 \times 10^{-10}$
	U-235	$< 2.5 \times 10^{-9}$
	K-40	$< 3.6 \times 10^{-6}$
CdZnTe	Th-232	$< 12 \times 10^{-9}$
	U-238	$< 41 \times 10^{-10}$
	U-235	$< 9 \times 10^{-9}$
	K-40	$< 8.4 \times 10^{-6}$
Delrin	Th-232	$< 12 \times 10^{-10}$
	U-238	$< 4 \times 10^{-10}$
	U-235	$< 4 \times 10^{-9}$
	K-40	$< 10 \times 10^{-7}$
Passivation Paint	Th-232	$(2.7 \pm 0.2) \times 10^{-7}$
	U-238	$(1.7 \pm 0.1) \times 10^{-7}$
	U-235	$(3.0 \pm 0.5) \times 10^{-7}$
	K-40	$(2.2 \pm 0.3) \times 10^{-4}$

Table 3  
Table of Systematics

Origin	Fractional contribution to half-life
Cd content	$\pm 0.02$
Deadlayer	$-0.009$
Crystal masses	$\pm 0.00015$
Detection Efficiency	$\pm 0.0002$
Background Subtraction	$\pm 0.0058$
Energy calibration	$\pm 0.02$
Total (quadratic)	$+0.029, -0.03$

Table 4  
Table of Background Counts Subtracted

Detector	Background	Uncertainty	Total Counts counts/(kg.day)	
			$^{113}\text{Cd}$	Uncertainty
2	1537.4	86.1	12630.3	91.9
3	1257.8	76.7	12166.9	99.8
5	1718.8	68.8	13440.2	94.4
7	1446.0	72.3	12497.1	85.8
8	2122.8	112.5	12777.0	138.9
9	1392.0	62.6	13157.9	111.5
10	1269.3	100.3	12018.5	92.4
11	1102.5	49.6	11678.7	108.6
12	1478.9	63.6	12670.8	115.7
14	1463.6	73.2	12380.8	85.2
15	1636.9	65.5	12980.3	90.9

Table 5  
Table of Results

Detector	Q keV	Uncertainty keV	Normalisation $\times 10^{-25}$	Uncertainty $\times 10^{-26}$	Fit range keV	Chi <sup>2</sup> /NDF
2	322.27	1.24	3.18	1.1	100–350	70.8/83
3	320.79	1.16	3.09	1.1	100–350	79.6/83
5	321.06	1.08	3.35	1.1	100–350	41.7/83
7	320.69	1.05	3.16	1.0	100–350	57.1/83
8	323.23	1.46	3.03	1.1	100–350	76.2/83
9	323.47	1.17	3.05	1.1	100–350	65.1/83
10	327.34	1.23	2.44	0.9	150–350	55.8/66
11	322.03	1.25	2.74	1.1	150–350	58.3/66
12	323.37	1.25	2.99	1.1	100–350	55.7/83
14	321.05	1.07	3.12	1.0	100–350	45.9/83
15	322.27	1.02	3.19	0.9	100–350	42.6/83

Table 6

Table of Results

Detector	Half-life (years)	Uncertainty (years)
2	$7.97 \times 10^{15}$	$0.35 \times 10^{15}$
3	$8.23 \times 10^{15}$	$0.38 \times 10^{15}$
5	$7.50 \times 10^{15}$	$0.30 \times 10^{15}$
7	$8.01 \times 10^{15}$	$0.32 \times 10^{15}$
8	$7.91 \times 10^{15}$	$0.45 \times 10^{15}$
9	$7.79 \times 10^{15}$	$0.34 \times 10^{15}$
10	$8.88 \times 10^{15}$	$0.44 \times 10^{15}$
11	$8.97 \times 10^{15}$	$0.47 \times 10^{15}$
12	$7.97 \times 10^{15}$	$0.38 \times 10^{15}$
14	$8.07 \times 10^{15}$	$0.32 \times 10^{15}$
15	$7.66 \times 10^{15}$	$0.32 \times 10^{15}$